Electronic Supplementary Information:

A new luminescent material $LaTiSbO_6:Mn^{4+}/Er^{3+}$ with high optical temperature sensing sensitivity based on fluorescence intensity ratio

Shen-Long Zhang, [a] Dan Zhao, [a, b*] Rui-Juan Zhang, [a] Qing-Xia Yao, [c*] Lei Jia, [a] Qiu Zong [a]

Table S1. The phosphor $LaTiSbO_6:xMn^{4+}/yEr^{3+}$ (x =0, 0.003; y= 0, 0.01, 0.03, 0.05, 0.07) detailed quantities (g) of raw materials.

Samples	x=0 y=0	x=0.003 y=0	x=0 y=0.05	x=0.003 y=0.01	x=0.003 y=0.03	x=0.003 y=0.05	x=0.003 y=0.07
La_2O_3(g)	1	1	0.95	0.9900	0.9700	0.9500	0.9300
TiO_2(g)	0.4903	0.4888	0.4903	0.4888	0.4888	0.4888	0.4888
Sb_2O_3(g)	0.8950	0.8950	0.8950	0.8950	0.8950	0.8950	0.8950
$MnCO_3$(g)	0	0.0021	0	0.0021	0.0021	0.0021	0.0021
Er_2O_3(g)	0	0	0.0593	0.0119	0.0356	0.0593	0.0830

The morphological and structural analysis of LTS:0.003Mn^{4+}/0.05Er^{3+} is shown in Fig. S1. It can be seen that the shape of the product is irregular and the elements La, Ti, Sb, O, Mn, and Er are uniformly distributed on the solid solution crystal.

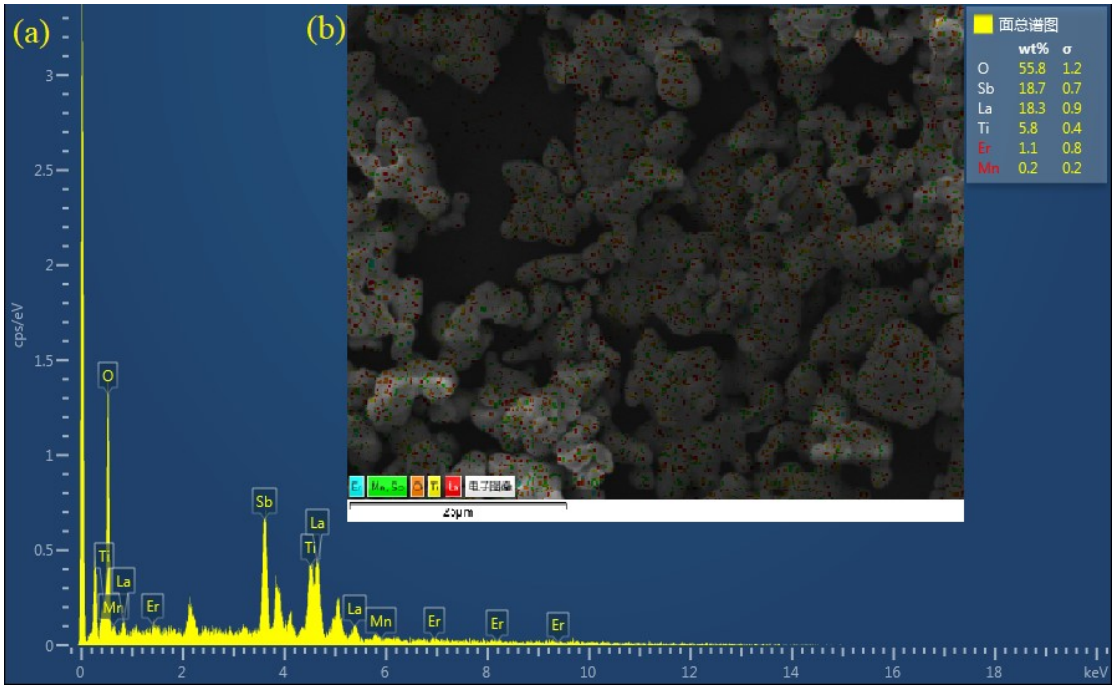

Figure S1. (a) element content analysis of La, Ti, Sb, O, Mn and Er; (b) element mappings of La, Ti, Sb, O, Mn and Er.

In Fig. S2a, the overall PLE spectrum can be fitted by Gaussian functions: 330 nm (30303.0 cm^{-1}), 366 nm (27322.4 cm^{-1}), 410 nm (24390.2 cm^{-1}), and 480 nm (20833.3cm^{-1}). By referring to works of literature, these bands can be assigned as follows: $O^{2-} \rightarrow Mn^{4+}$ charge transfer at 330 nm, $^4A_{2g} \rightarrow {}^4T_{1g}$ transition at 366 nm (spin allowed), $^4A_{2g} \rightarrow {}^2T_{2g}$ transition at 410 nm (spin forbidden), and $^4A_{2g} \rightarrow {}^4T_{2g}$ transition at 480 nm (spin allowed). Furthermore, the photoluminescence emission (PL) band centered at 684 nm by using 342 nm as an exciting source due to the transition of Mn^{4+} from the ^2E_g to $^4A_{2g}$ state.[1-4]

$$D_q = \frac{E(^4A_{2g} \rightarrow {}^4T_{2g})}{10} \quad (1)$$

$$\frac{D_q}{B} = \frac{15(x-8)}{(x^2-10x)} \quad (2)$$

$$x = \frac{E(^4A_{2g} \rightarrow {}^4T_{1g}) - E(^4A_{2g} \rightarrow {}^4T_{2g})}{D_q} \quad (3)$$

$$\frac{E(^2E_g \rightarrow {}^4A_{2g})}{B} = \frac{3.05C}{B} - \frac{1.8B}{D_q} + 7.9 \quad (4)$$

According to Eqs. (1)– (4), the values of D_q, B, and C for LTSO: 0.003Mn^{4+} are determined to be 2083.3, 609.69, and 3319.7 cm^{-1}, respectively. The ratio of D_q to B, which is 3.416, exceeds the threshold of 2.2, indicating that the LTS: 0.003Mn^{4+} phosphor has a strong crystal field effect.

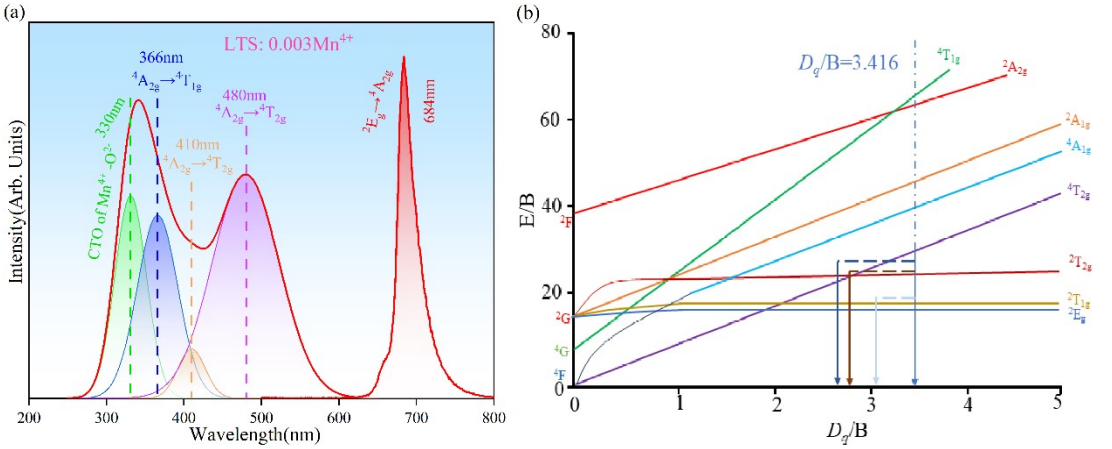

Figure S2. (a) Multi-peaks Gaussian fitting; (b) Tanabe-Sugano energy-level diagram.

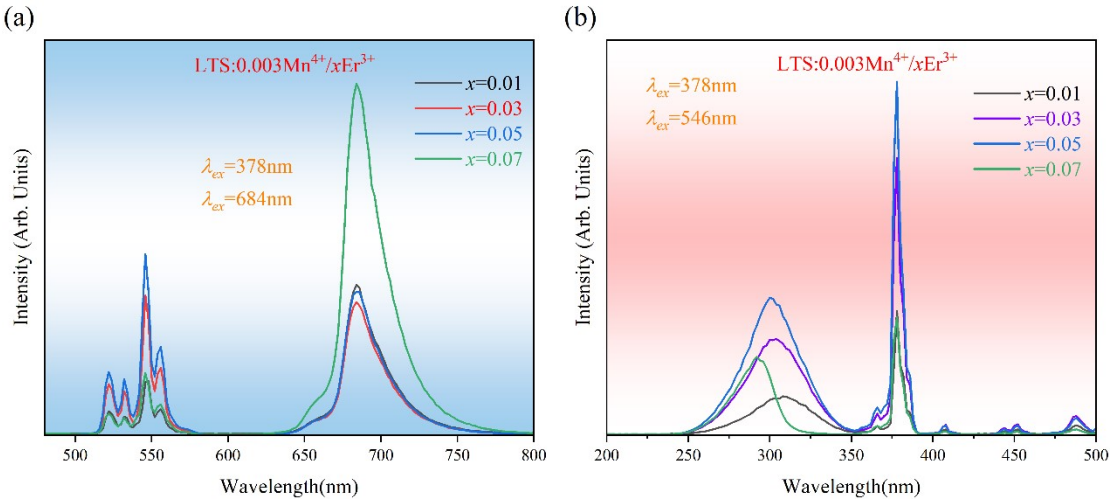

Figure S3. (a)PL spectra of the as-prepared LTS:0.003Mn^{4+}/xEr^{3+} (x = 0.01, 0.03, 0.05, 0.07) with different concentrations under excitation of 378 nm. (b)PLE spectra of the as-prepared LTS:0.003Mn^{4+}/xEr^{3+} (x = 0.01, 0.03, 0.05, 0.07) with different concentrations under excitation of 378 nm.

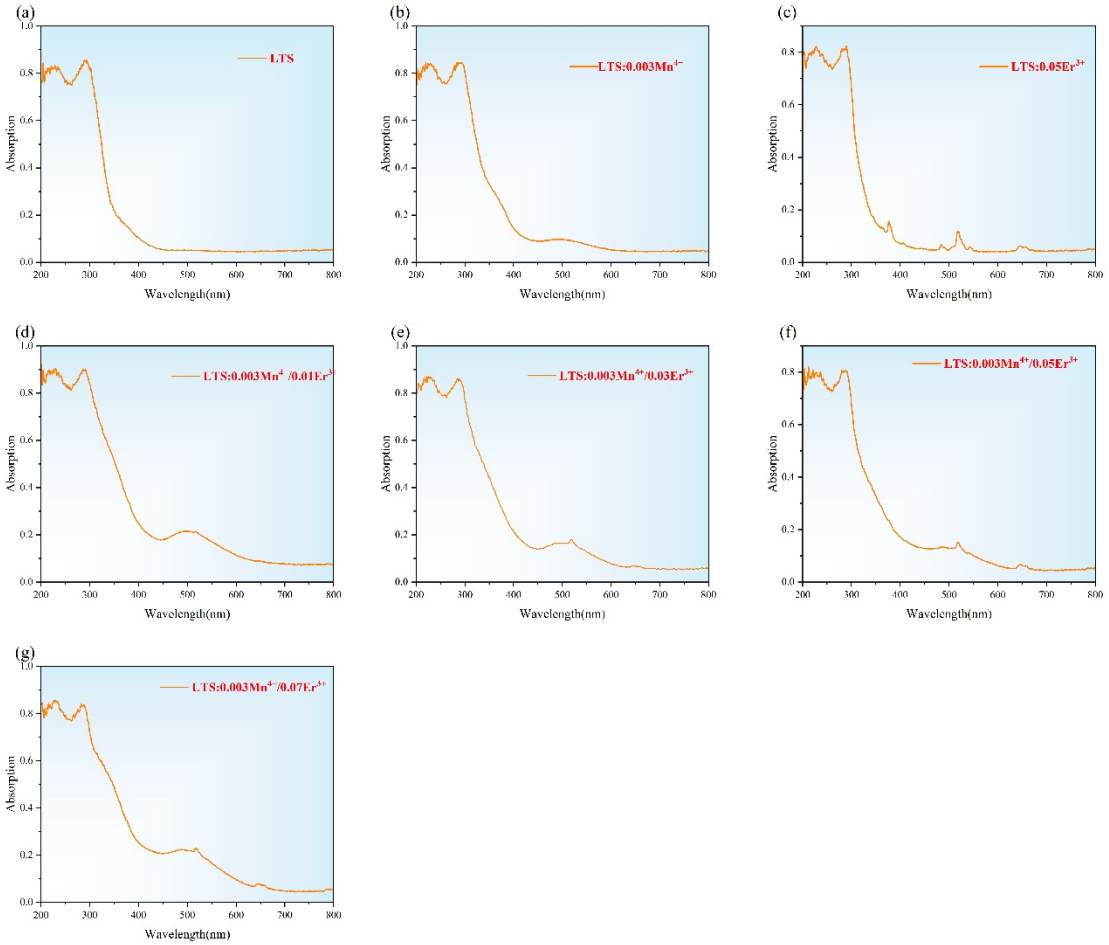

Figure S4. (a-g) Ultraviolet absorption spectroscopy of LTS, LTS:0.003Mn^{4+}, LTS:0.05Er^{3+}, LTS:0.003Mn^{4+}/0.01Er^{3+}, LTS:0.003Mn^{4+}/0.03Er^{3+}, LTS:0.003Mn^{4+}/0.07Er^{3+} and LTS:0.003Mn^{4+}/0.07Er^{3+}.

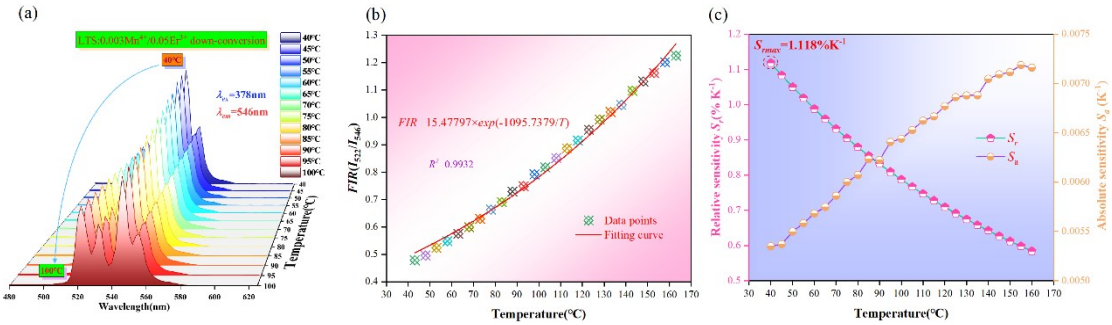

Figure S5. (a) The temperature-dependent photoluminescence spectra of the Er^{3+} thermal coupling peak in LTS:0.003Mn^{4+}/0.05Er^{3+} from 40 to 100 ℃; (b) Varying of emission intensity ratio (I_{522}/I_{546}) with temperature from 40 to 160 ℃;(c) Relative sensitivity S_r (left) and S_a (right) in the range of 40 to 160 ℃.

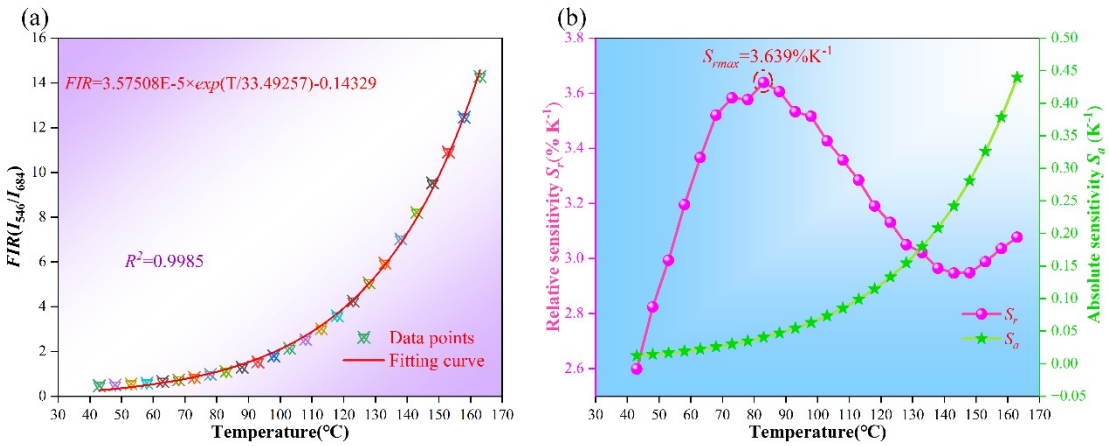

Figure S6. (a) Varying of emission intensity ratio (I_{546}/I_{684}) with temperature from 40 to 160 ℃; (b) Relative sensitivity S_r (left) and S_a (right) in the range of 40 to 160 ℃.

The temperature-dependent PL of LTS:0.003Mn^{4+}/0.05Er^{3+} from 40 to 100 °C was studied under 980 nm excitation, as described in Fig. S7a. The UC emission from Er^{3+} consisted of two green luminescence peaking at 522 nm ($^2H_{11/2}\rightarrow{}^4I_{15/2}$) and 546 nm ($^4S_{3/2}\rightarrow{}^4I_{15/2}$) and red emission peaking at 657 nm corresponding to $^4F_{9/2}\rightarrow{}^4I_{15/2}$. Within the temperature range of 40 to 100 °C, the intensity of the emission peaks gradually decreases as the temperature increases. By using equations (3), the *FIR* values can be calculated at each temperature, which is presented in Fig. S7b. The *FIR* values increase from 0.3537 to 0.89787 from 40 to 160 °C. Using equations (4) and (5), The highest values S_a and S_r are 0.0050 K^{-1} at 160 °C and 1.058% K^{-1} at 40 °C, which is presented in Fig. S7c.

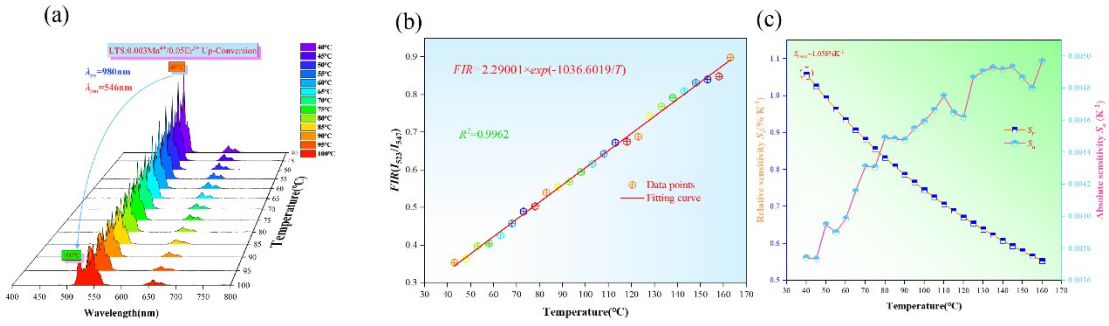

Figure S7. (a) The temperature-dependent photoluminescence spectra of the Er^{3+} thermal coupling peak in LTS:0.003Mn^{4+}/0.05Er^{3+} from 40 to 100 ℃; (b) Varying of emission intensity ratio (I_{522}/I_{546}) with temperature from 40 to 160 ℃;(c) Relative sensitivity S_r (left) and S_a (right) in the range of 40 to 160 ℃.

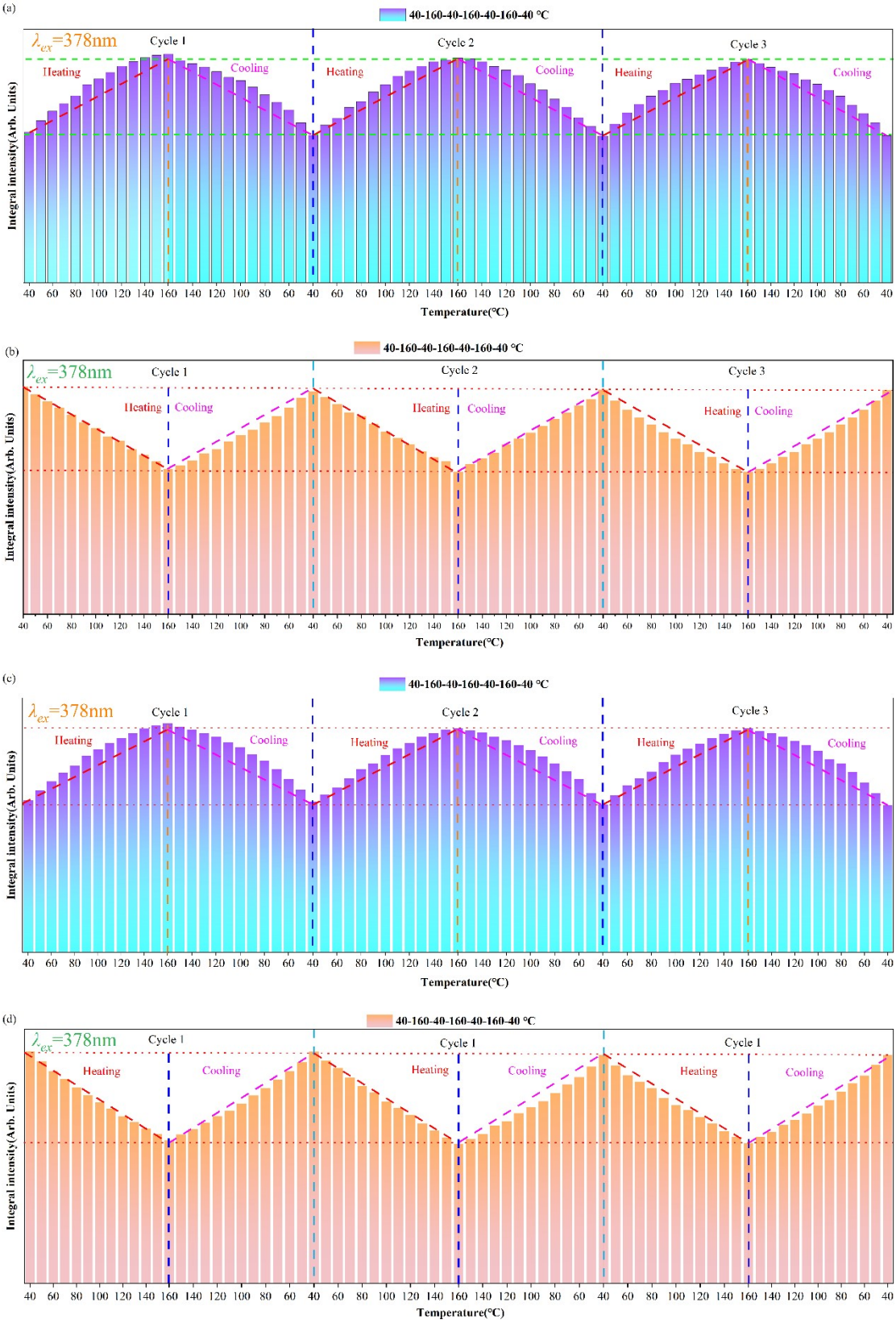
(a)
40-160-40-160-40-160-40 ℃
λex=378nm
Cycle 1
Cycle 2
Cycle 3
Heating
Cooling
Integral intensity(Arb. Units)
Temperature(℃)
(b)
40-160-40-160-40-160-40 ℃
λex=378nm
Cycle 1
Cycle 2
Cycle 3
Heating
Cooling
Integral intensity(Arb. Units)
Temperature(℃)
(c)
40-160-40-160-40-160-40 ℃
λex=378nm
Cycle 1
Cycle 2
Cycle 3
Heating
Cooling
Integral intensity(Arb. Units)
Temperature(℃)
(d)
40-160-40-160-40-160-40 ℃
λex=378nm
Cycle 1
Cycle 1
Cycle 1
Heating
Cooling
Integral intensity(Arb. Units)
Temperature(℃)

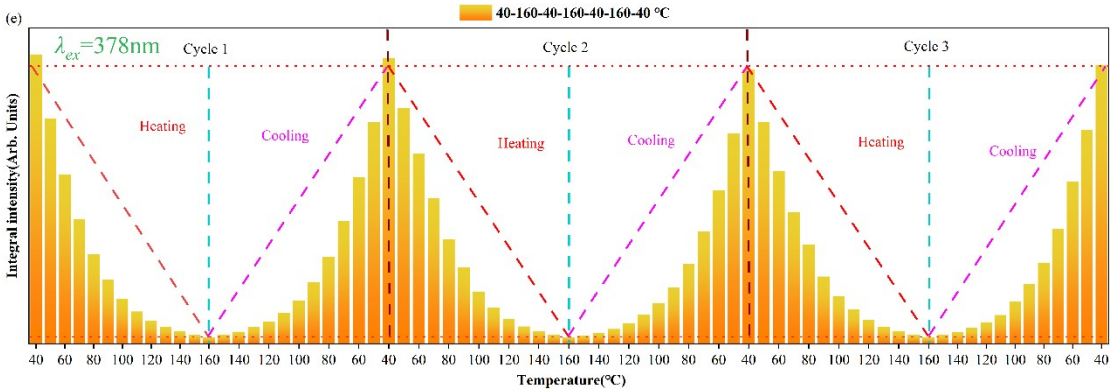

Figure S8. (a) Varying of the LTS:0.05Er^{3+} 522 emission peaks intensity for periodic cycles; (b) Varying of the LTS:0.05Er^{3+} 546 emission peaks intensity for periodic cycles; (c) Varying of the LTS:0.003Mn^{4+}/0.05Er^{3+} 522 emission peaks intensity for periodic cycles; (d) Varying of the LTS:0.003Mn^{4+}/0.05Er^{3+} 546 emission peaks intensity for periodic cycles; (e) Varying of the LTS:0.003Mn^{4+}/0.05Er^{3+} 684 emission peaks intensity for periodic cycles.

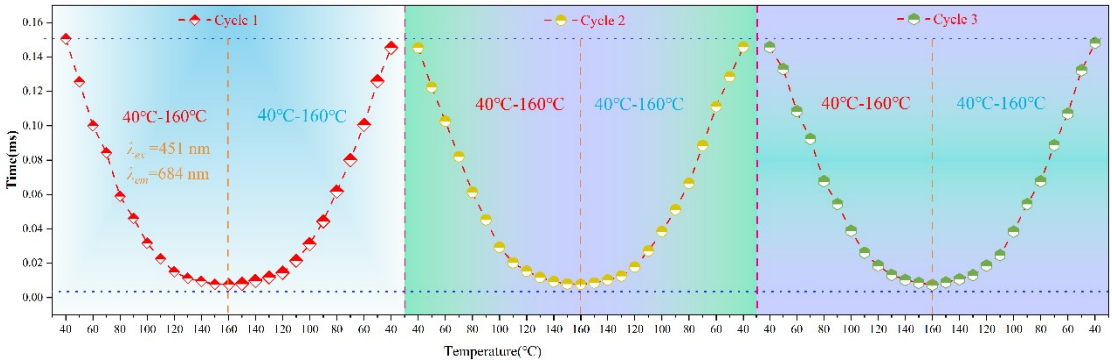

Figure S9. Varying of the LTS:0.003Mn^{4+}/0.05Er^{3+} lifetime for periodic cycles.

Notes and references

1.Y. Chen, F. Liu, Z. Zhang, J. Hong, M. S. Molokeev, *J. Mater. Chem. C* 2022, **10** (18), 7049-7057.

2.T. Lv, J. Huang, C. Yang, Y. Wang, Q. Huang, J. Chen, W. Guo, *J. Mater. Chem. C* 2022, **10** (26), 9773-9785.

3.T. Wanjun, D. Shuang, Y. Yuhong, *J. Lumin.* 2019, **215**, 116650.

4.R. Cao, X. Ouyang, Y. Jiao, X. Wang, Q. Hu, T. Chen, C. Liao, Y. Li, *J. Alloys Compd.* 2019, **795**, 134-140.